RSC Advances

ROYAL SOCIETY OF CHEMISTRY

www.rsc.org/advances

ARTICLE TYPE www. rsc.org/xxxxxx | XXXXXXXX

Unexpected Surface Superparamagnetism in Antiferromagnetic Cr_2O_3 Nanoparticles

Zhaolong Yang,[a] Jing Zhang,[a] Daqiang Gao,[a] Zhonghua Zhu,[b] Guijin Yang,[c] and Desheng Xue*[a]

Received Xth XXXXXXXXXX 20XX, Accepted Xth XXXXXXXXX 20XX
First published on the web Xth XXXXXXXXXX 200X
DOI: 10.1039/b000000x

We report an unexpected superparamagnetic behavior in antiferromagnetic Cr_2O_3 nanoparticles. The Cr_2O_3 particle cores retain their original antiferromagnetic phase, while the surfaces of the particles become superparamagnetic. The X–ray diffraction results confirm that the sample is corundum structure without any other phases. Through X–ray photoelectron spectroscopy characterizations, the particle surfaces present three different oxidation states: Cr^{3+} (antiferromagnetic), Cr^{4+} (ferromagnetic), and Cr^{6+} (nonferromagnetic). A bimagnetic particle model with Cr^{3+} cores and higher Cr oxidation surface states is given to explain the experimental results. In addition, we observe that spin–flop transition occurs in the antiferromagnetic cores below the Néel temperature (292 K). The spin–flop transition field is uncommon comparing with other research, this novel behavior is attributed to the presence of superparamagnetism in the surfaces through the exchange field. These findings reveal the significance of surface states in mediating magnetic properties in antiferromagnetic materials.

1 Introduction

Due to its important applications in exchange bias and spin–valve devices, antiferromagnetic (AF) oxides have been intensively investigated.[1–3] Special types of bimagnetic particles with core/shell structure receive more attention: each CrO_2 particle is enclosed by a Cr_2O_3 layer, which is unexpected for ferromagnetic (FM)/AF core/shell structured particles;[4] the magnetic properties of an AF MnO core and a FM passivation shell (γ-Mn_2O_3 or Mn_3O_4) had been investigated;[5] the core behaves as a regular antiferromagnet and the shell becomes a two-dimensional diluted antiferromagnet in Co_3O_4 nanowires;[6] in NiO nanoparticles, the core retains its original AF order while the shell behaves as a spin glass system (Ni^{3+} ions).[7,8]

Cr_2O_3, as a typical AF material, has received increased attention because of its abundant magnetic properties. Below the Néel temperature (T_N = 308 K)[4,9,10] in zero magnetic field, the Cr^{3+} spins align antiferromagnetically along the [111] easy axis.[7] Because of the AF order of the spins, the crystal loses both space– and time–reversal symmetry below T_N, this symmetry reduction leads to that in sufficiently high magnetic fields along the z axis the spins flop into the basal plane maintaining their AF order, which is called as spin–flop (SF). SF is a first-order transition that occurs at a critical field (H_{SF}; H_{SF} = 5.8 T below 90 K).[9] Up to now, most groups had observed the SF transition experimentally at sufficiently high magnetic fields in low temperature range;[10,11] Among those, Foner *et. al.* systematically investigated the H_{SF} of Cr_2O_3 and $(Cr_2O_3)_{0.9}\cdot(Al_2O_3)_{0.1}$ from 4.2 K to about $0.95T_N$,[12] which significantly broaden the temperature range where the SF transition happens comparing with other experimental or theoretical conclusions.

In this paper, we report an unexpected superparamagnetic (SPM) behavior in AF Cr_2O_3 nanoparticles, the SPM signals could even exist above T_N. Magnetic properties of the bimagnetic nanoparticles with AF cores and SPM surface states are studied and the origin of the anomalous magnetic behavior is discussed in detail. More interestingly, the presence of SPM surface state influences the AF core, which makes that the behavior of H_{SF} in AF phase is unusual comparing with other research.[9–12]

2 Experimental Section

2.1 Synthesis of Cr_2O_3 Nanoparticles

The chemical reagent used as starting material is analytical grade and were used without any further treatment. Cr_2O_3 nanoparticles were synthesized by thermal decomposition of chromium chloride hexahydrate ($CrCl_3\cdot6H_2O$). The starting material was sintered at 800 °C for 1 hr in the air to obtain the sample. As–prepared Cr_2O_3 nanoparticles were annealed in oxygen atmosphere (Cr_2O_3–O_2) at 500 °C for 1 hr to study the origin of the magnetism.

[a] *Key Laboratory for Magnetism and Magnetic Materials of MOE, Lanzhou University, Lanzhou 730000, P. R. China. Fax: +86-0931-8914160; Tel: +86-0931-8912237; E-mail: xueds@lzu.edu.cn*
[b] *Hunan University of Science and Technology, Xiangtan 411201, P. R. China.*
[c] *College of Physics and Electronic Engineering, Northwest Normal University, Lanzhou 730070, P. R. China.*

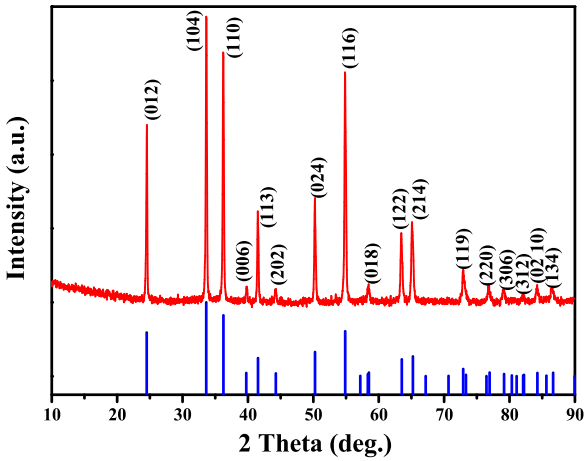

Fig. 1 XRD pattern of Cr_2O_3 nanoparticles, together with the theoretical pattern of Cr_2O_3 in corundum structure [rhombohedral lattice system with space group of $R\bar{3}c$(167), JCPDS card No. 84–1616].

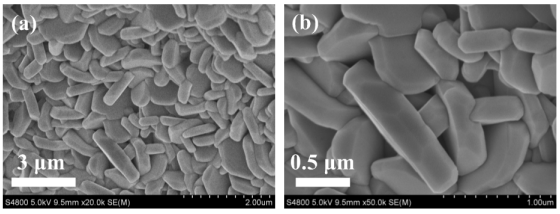

Fig. 2 (a), (b) SEM images of Cr_2O_3 nanoparticles. The nanoparticles aggregate to form microplates.

2.2 Characterization

X–ray diffraction (XRD; X'Pert PRO PHILIPS with Cu K_α radiation, Almelo, Netherlands) was employed to study the structure of the sample. The morphology was characterized by scanning electron microscope (SEM; Hitachi S–4800, Chiyoda–ku, Japan). Microstructure of the sample was obtained using a transmission electron microscope (TEM; Tecnai TMG2F30, FEI) and high–resolution TEM (HRTEM) equipped with energy dispersive X–ray spectrometer (EDX). Measurements of magnetic properties were performed using a Quantum Design MPMS magnetometer based on a superconducting quantum interference device (SQUID; Quantum Design, Inc., San Diego, USA). X–ray photoelectron spectroscopy (XPS; VG Scientific ESCALAB–210 spectrometer, East Grinstead, UK) was utilized to determine the bonding characteristics and the composition of the nanoparticles.

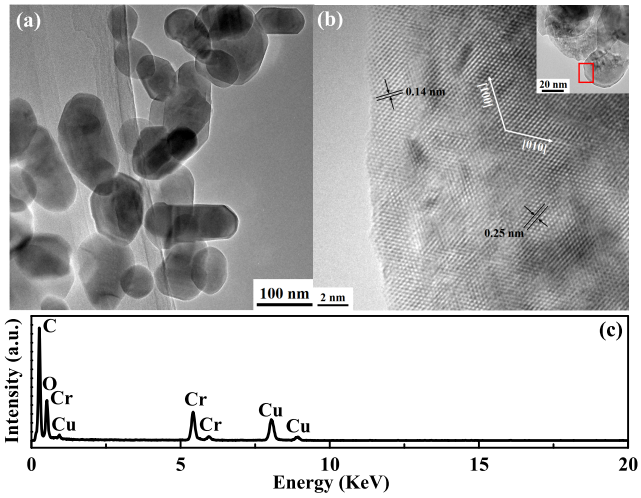

Fig. 3 (a) TEM image of Cr_2O_3 nanoparticles. (b) High resolution TEM image of Cr_2O_3 nanoparticles, the interplanar spacing of (110 is 0.25 nm. Inset shows the region where the HRTEM image is obtained. (c) Corresponding EDX result of Cr_2O_3 nanoparticles.

3 Results and Discussion

The XRD pattern of Cr_2O_3 nanoparticles is shown in Fig. 1. The results indicate that the sample is corundum structure [rhombohedral lattice system with space group of $R\bar{3}c$(167), JCPDS card No. 84–1616, a = b = 4.97 Å, c = 13.67 Å] without any other phases. SEM images (Fig. 2) reveal that the sample is formed of aggregated microplates with 0.2 $\sim$ 0.4 μm thickness and 1 $\sim$ 4 μm radius. In order to see the size of crystallites which aggregated into microplates, the sample was measured by TEM after a longtime ultrasonic treatment. As shown in Fig. 3(a), the sample dispersed into small particles after ultrasonic treatment. The particle diameters distribute in the range of 60 $\sim$ 80 nm. On the other hand, using the Scherrer formula for the full width at half–maximum of the main peaks in XRD pattern, the average crystallite size is calculated to be 68.3 $\pm$ 3.9 nm which matches the particle size read from Fig. 3(a) well. From the HRTEM image shown in Fig. 3(b), the clear atom arrangement can be found inside of the particle, and the representative interplanar spacing is 0.25 nm equaling to the (110) plane of Cr_2O_3. Fig. 3(c) depicts the corresponding EDX result of our sample, only the elements Cr, O, Cu, and C are present. It can be understood that Cu and C are from the carbon membranes which hold the sample during measurement. Besides, none of impurity element was detected.

Figure 4(a) shows the zero–field–cooled (ZFC) and field-cooled (FC) magnetization curves. It is worth noting that two temperature peaks are observed: the first broad one (T_{p1}) at around 91 K and the second one (T_{p2}) at about 292 K. Whe

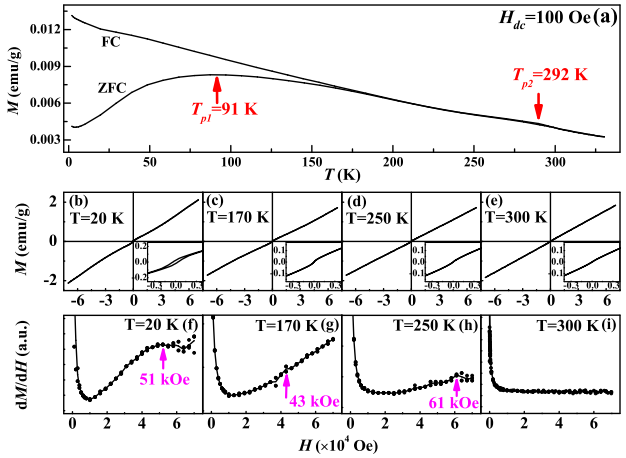

Fig. 4 (a) ZFC–FC curves at the dc field of 100 Oe in the temperature range of 2 ∼ 330 K. *M–H* curves at several temperatures [(b) 20 K, (c) 170 K, (d) 250 K, (e) 300 K]. The magnification of the central part for *M–H* curves are shown in insets. The SF transition is indicated by the change of curvature in the *M–H* curves. Numerical derivative of the *M–H* curves are shown in (f) 20 K, (g) 170 K, (h) 250 K, (i) 300 K.

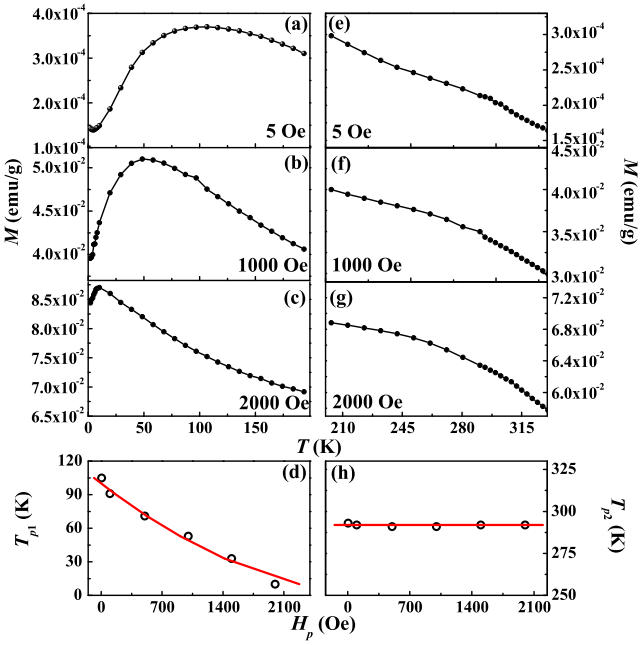

Fig. 5 Field dependence of ZFC curves at (a), (e) 5 Oe; (b), (f) 1000 Oe; (c), (g) 2000 Oe. (d), (h) Plots of T_{p1} and T_{p2} vs H_p (black circles); red line shows the fitting results.

cooling down from 330 K, ZFC and FC curves overlap closely until a peak at 292 K appears in both curves. Then they follow a similar trend, that is, the susceptibility increases slowly with the decreasing temperature. Below T_{p1}, the dividable curves reveal that the magnetization reversal is irreversible. We also measured magnetization curves as a function of applied magnetic field (*M–H*) at different temperatures [Fig. 4(b) ∼ (e)]. The curves after deducting the AF contribution are shown in Fig. S3. It can be seen that all the *M–H* curves show an S–shape signal in lower field (< 0.5 T), and the curves measured below T_{p2} show a nonlinear behavior with the increasing of magnetization in higher field (> 2 T). The latter one is the characteristic of SF transition. In order to further study S-F transition, we have performed the numerical derivative of the *M–H* curves, and H_{SF} is defined as the maximum in the derivative curves in the Fig. 4(f) ∼ (i). The SF transition is observed from 20 K to 250 K and H_{SF} decreases firstly, then increases with the rise of measuring temperature: the corresponding H_{SF} is 5.1, 4.3, and 6.1 $\times 10^4$ Oe at 20, 170, and 250 K, respectively. This phenomenon is different from those reported earlier: the H_{SF} increased monotonously with increase of the critical temperature,[10,12] and that will be discussed in detail below.

The moments after deducting the AF signal at 300 K [Fig. S3(h)] yield the clear S–shape dependence of the applied magnetic field. Remarkably, no coercivity is found, which might betoken appearance of superparamagnetism. In fact, from the magnification of the central part of *M–H* curves measured at 20 K below T_{p1} [the inset of Fig. 4(b)] and 170 K between T_{p1} and T_{p2} [the inset of Fig. 4(c)], it can be clearly seen that coercivity exists at 20 K while it is absent at 170 K. Those suggest that T_{p1} might be the particle blocking temperature (T_B) of the SPM system. In order to further explore the origin of T_{p1} and T_{p2}, the ZFC magnetization curves were taken under different magnetic fields (Fig. 5). The T_{p1} (< 150 K) shifts to lower temperature side with the increasing magnetic field. The cusp temperature under different magnetic fields obeys the relationship ${H_{p1}}^2 \propto (1–T_{p1})$, and the curve of T_p vs H_p [where T_{p1} is defined as the maximum in the Fig. 5(a) ∼ (c)] is shown in Fig. 5(d), which is expected for a SPM system.[13–15] These results confirm the above conclusions about superparamagnetism based on the *M–H* curves at different temperatures. As shown in Fig. 5(e) ∼ (g), where T_{p2} is defined as the inflection point of each curve, there is distinct difference between the plots of T_{p2} from T_{p1} vs H_p. The plateau where $T_{p2} \sim 292$ K appears [Fig. 5(h)] in contrast to the sharp decrease of T_{p1} with the decreasing H_p. In most AF systems, the field dependence of the critical phase boundary is very small in the range of the usually accessible experimental field values.[16] Therefore, we can conclude that the T_{p2} is the AF phase transition temperature (T_N). The T_N of our AF Cr_2O_3 particles is reduced in comparison with the bulk value (308 K)[4,9,10], which would be the result of the decrease in particle size.[10,16]

It is common to observe hysteresis loops and divergence between ZFC/FC curves in low dimension AF materials. How

ever, there is no recognized explanation to solve these problems until now. Different models are built in each AF system. Presence of an AF core and a ferromagnetic passivation shell was proposed in investigating the magnetic properties of MnO nanoparticles.[5] It is found that γ-Mn_2O_3 or Mn_3O_4 (depends on the particle size) would present in the particle shell due to the surface passivation. Benitez *et. al.* attributed the irreversible magnetization of AF Co_3O_4 nanowires to the wire shells which form two–dimensional diluted AF systems.[6] This model also applies to AF $BiFe_{0.8}Mn_{0.2}O_3$ nanoparticles.[17] The picture is more complicated for NiO system. Claims such as presence of Ni^{3+} ions within the AF NiO lattice,[18] AF interaction with canted surface spins,[3] or surface spin disorder induced spin–glass behavior rather than SPM[19] were proposed to explain the anomalous magnetic properties in NiO nanoparticles. In our system, the unexpected SPM behavior and spin-flop (SF) transition have been observed. Specifically, the SPM signals could exist above T_N of Cr_2O_3, which means the magnetic coupling of that SPM cannot be the superexchange among Cr^{3+}–O^{2-}–Cr^{3+}. What is the origin of superparamagnetism in AF Cr_2O_3 particles? How to generate net moments in this AF system? Many different mechanisms based on the origin of moments have been proposed in the oxide systems: 1) Defects bear the brunt of the origin, especially O vacancies: CuO (O vacancies),[20] CoO (O vacancies);[21] 2) The mixed valences could cause ferromagnetism, such as, CeO_2 (the surface Ce^{3+}/Ce^{4+} pairs),[22] VO_2 (the valence charge defects with unpaired electrons V^{5+} in VO_2 thin film).[23] In order to further identify the origin of moments in our system, Cr_2O_3–O_2 samples were prepared. The *M–H* curve of Cr_2O_3–O_2 is shown in Fig. S5 (red line). The hysteresis loops of two samples are similar, which indicates that the observed SPM should not be directly related with O vacancies.

The chemical states of the compositional elements in Cr_2O_3 particles were revealed by the XPS. In Fig. 6, the survey spectrum, the indexed peaks only correspond to elements Cr, O, and C, where the binding energies are calibrated by taking carbon C 1*s* peak (285.0 eV). The peak in the Cr $2p_{3/2}$ spectrum (the inset of Fig. 6) is not totally symmetrical, which can be well fitted by three peaks with different binding energy components:[24] The dominant peak located at 577.2 eV is assigned to Cr^{3+} ions; the other binding energy components can match Cr^{4+} ions (576.3 eV) and Cr^{6+} ions (579.0 eV). It is common to see the presence of a higher oxidation state at the surface of the transition metal oxides which have several stable oxidation states due to surface effect. For example, in epitaxial undoped VO_2 thin films which are grown by pulsed laser deposition, different valence states of V ions were found at the surface by XPS characterization.[23] The major part of that is a higher oxidation state (V^{5+}) and takes up 47% of the V ions. Another example is AF MnO nanoparticles, the Mn ions at

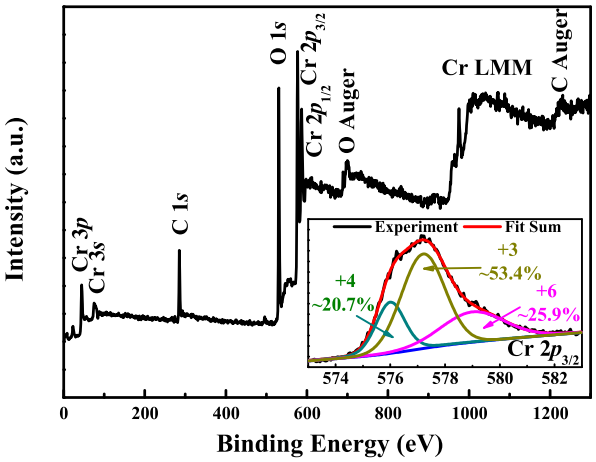

Fig. 6 XPS survey spectrum. The inset shows high resolution scan and fitting results of Cr $2p_{3/2}$ core level.

the particle surface are oxidized to a higher valence (Mn^{3+}) due to the passivation effect and form a surface passivation shell of γ–Mn_2O_3 or Mn_3O_4.[5] Similarly, the surface of the as–grown CoO nanoparticles appears oxidized up to Co_3O_4, and the surface effects here are described as a large amount of point defects which adsorb mainly oxygen species.[25] Valence states of +2, +3, +4, and +6 are familiar in Cr ions, and our samples are synthesized in the air. Therefore it is possible to present higher oxidation states of Cr ions than "+3" at the particle surfaces. Reddy *et. al.* investigated magnetic coupling of Cr_2O_n (n = 1 $\sim$ 6) and found that the moments at the Cr sites in Cr_2O_3 are antiferromagnetically coupled; the moments at the two Cr sites in CrO_2 are ferromagnetically coupled ($T_C \approx 396$ K); while the Cr sites have negligible moment in CrO_3.[26] Thus, we further consider that the appearance of SPM in Cr_2O_3 nanoparticles is owing to the presence of Cr^{4+} surface state rather than O vacancies.

As discussed above, the anomalous behavior of the ZFC curve [Fig. 4(a)] could be explained by the formation of a Cr_2O_3 core with CrO_2 surface state system: the moments (FM CrO_2 surface) of the particles are blocked below the T_B ($\sim$ 91 K), and SPM above T_B; the kinks at 292 K in the curve must be caused by the order/disorder transition of the AF Cr_2O_3 cores.[13] Néel predicted that AF material in fine particle form should exhibit some interesting magnetic properties including superparamagnetism and a weak ferromagnetism, which has been also observed in various AF particles as the particle size decreases. As the particle size decreases, a net magnetic moment is produced due to the nonexact compensation of the two magnetic sublattices, for example, imbalance in the number of "up and down" spins. A SPM susceptibility, due to uncompensated spins, can dominate over the AF contribution itself.[11,27,28] In the synthesized Cr_2O_3 nanoparticles (Fig

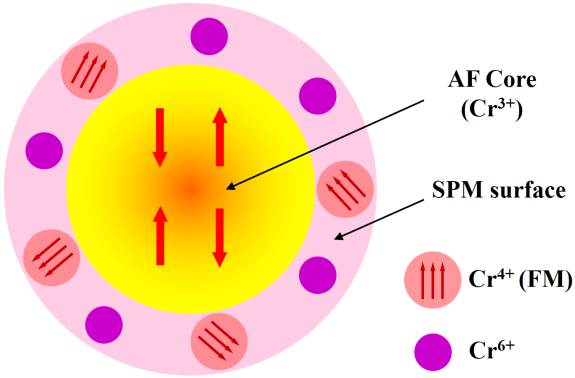

Fig. 7 A schematic diagram (red arrows represent the spins). For Cr_2O_3 nanoparticles, the core (inside circles) spins are almost antiparallel; in the surface, there is the mixture of Cr^{6+} clusters with negligible moments and Cr^{4+} clusters which are so small that superparamagnetism appears.

7), we also observed the similar results: the cores show regular AF orders, whereas the surface exhibits superparamagnetism from the symmetry breaking of surface Cr^{4+} cations (as well, Cr^{6+} cations have negligible moments). These results are similar to previous studies on Co_3O_4 nanostructures and MnO nanoparticles, where AF systems are usually governed by core–shell behavior.[5,16]

The SF phenomenon as a kind of striking nonlinear effects in antiferromagnets is observed when H equals a critical field H_{SF} given by:[10,12]

$$H_{SF}^2 = \frac{2H_E H_A}{1 - \chi_{\parallel}/\chi_{\perp}} \quad (1)$$

where H_E is the exchange field in the molecular–field approximation for two AF coupled sublattices, H_A is the anisotropy field, $\chi_{\parallel}$ and $\chi_{\perp}$ are the parallel and perpendicular susceptibilities respectively. It is interesting that H_{SF} in our sample is much lower than other reports,[10,12] which should be related to appearance of the SPM phase. Bhowmik *et. al.* gave the model about AF orders of spins in bulk and nanoscale samples:[27] 1) The long range AF interactions for the perfect bulk sample spans up to many particles without any modulation ($H_{Ecore} = H_{Eshell}$); 2) For nanoparticles, the core spins are almost antiparallel with slight distortion near the shell and the deviation of shell spins from the AF arrangement makes the H_E value become less negative in the shell regions. Similarly, in our bimagnetic nanoparticles $H_{Ecore} < H_{Eshell} < 0$ due to the appearance of surface moments. The smaller absolute value of H_E causes lower H_{SF} compared with other Cr_2O_3 bulk systems.

Furthermore, through the molecular–field constant λ and the hypothesis that $\chi_{\perp} \sim 1/\lambda$ when $H_E \gg H_A$, equation (1) transforms into:[10–12]

$$H_{SF}^2 = \frac{2K}{\chi_{\perp} - \chi_{\parallel}} \quad (2)$$

where K is the anisotropy constant which saturates in low temperature range;[29] the perpendicular susceptibility $\chi_{\perp}$ is independent on temperature, and the parallel susceptibility $\chi_{\parallel}$ decreases as temperature decreases and vanishes at 0 K.[30,31] As can be seen, the SF transition provides information of the anisotropy, which in an AF system is generally difficult to be obtained through other experiments.[10] It is also worth remarking that in all Cr_2O_3 bulk and particle systems H_{SF} increases when the temperature rises monotonously.[10,12] This dependence is a characteristic for AF systems because the difference $(\chi_{\perp} - \chi_{\parallel})$ decreases faster than the magnetic anisotropy constant K when the temperature increases.[10,30,31] However, it is puzzling in our system that the observed behavior of $H_{SF}(T)$ is nonmonotonic, especially the increase of H_{SF} below T_B. At room temperature or any temperature above T_B, the SPM part has sufficient thermal energy to overcome the energy barrier and thus the magnetic spins are free to fluctuate between orientations owning to both applied magnetic field H and the AF core; below T_B, the spins are frozen, or blocked, along their anisotropy axis resulting in a disordered state common to SPM one.[32] In addition, we expect that our observations will become more pronounced with the decreasing crystallite size. The unexpected SPM signal is attributed to the presence of Cr^{4+} at particle surface. Just like the anomalous magnetic behavior which has been investigated in other low–dimensional AF systems, it can be expected that the one associated with surface effect would further enhance with the decreasing scale of system due to the higher surface to volume ratio.[3,5,7,19,25,33] Similarly, the AF anisotropy will be weakened with the decreasing particle size, which leads that the magnetization reversal becomes more easily under applied field keeping the antiparallel arrangement of spins. Then the SF transition might be observed in lower field.

4 Conclusions

In summary, bimagnetic Cr_2O_3 nanoparticles with corundum structure were directly synthesized by thermal decomposition. SF transition in the AF core occurs below T_N (292 K), and appearance of SPM surface state is owing to the valence increase (Cr^{4+} state). In addition, SPM surfaces make influence on the inside AF cores through the exchange field, which leads to the increase of H_{SF} below T_B. We hope our work could give an insight into the magnetic properties of Cr_2O_3 nanoparticles and provide a path to control magnetic ordering in AF materials.

ACKNOWLEDGEMENTS

This work is supported by National Science Fund for Distinguished Young Scholars (Grant Nos. 50925103 and 11034004), the Keygrant Project of Chinese Minisity of Education (Grant No. 309027), and NSFC (Grant No.50902065).

References

1 B. Dieny, V. S. Speriosu, S. Metin, S. S. P. Parkin, B. A. Gurney and P. Baumgart, *J. Appl. Phys.*, 1991, **69**, 4774.
2 V. Skumryev, S. Stoyanov, Y. Zhang, G. Hadjipanayis, D. Givord and J. Nogues, *Nature (London)*, 2003, **423**, 850–853.
3 J. B. Yi, J. Ding, Y. P. Feng, G. W. Peng, G. M. Chow, Y. Kawazoe, B. H. Liu, J. H. Yin and S. Thongmee, *Phys. Rev. B*, 2007, **76**, 224402.
4 R. K. Zheng, H. Liu, R. K. Zheng, H. Liu, Y. Wang and X. X. Zhang, *Appl. Phys. Lett.*, 2004, **84**, 702–704.
5 A. López-Ortega, D. Tobia, E. Winkler, I. V. Golosovsky, G. Salazar-Alvarez, S. Estradé, M. Estrader, J. Sort, M. A. González, S. Surinach, J. Arbiol, F. Peiró, R. D. Zysler, M. D. Baró and J. Nogués, *J. Am. Chem. Soc.*, 2010, **132**, 9398–9407.
6 M. J. Benitez, O. Petracic, E. L. Salabas, F. Radu, H. Tüysüz, F. Schüth and H. Zabel, *Phys. Rev. Lett.*, 2008, **101**, 097206.
7 S. Mandal, S. Banerjee and K. S. R. Menon, *Phys. Rev. B*, 2009, **80**, 214420.
8 M. Ghosh, K. Biswas, A. Sundaresan and C. N. R. Rao, *J. Mater. Chem.*, 2006, **16**, 106–111.
9 M. Fiebig, D. Fröhlich and H. J. Thiele, *Phys. Rev. B*, 1996, **54**, R12681–R12684.
10 D. Tobia, E. Winkler, R. D. Zysler, M. Granada and H. E. Troiani, *Phys. Rev. B*, 2008, **78**, 104412.
11 R. D. Zysler, D. Fiorani, A. M. Testa, L. Suber, E. Agostinelli and M. Godinho, *Phys. Rev. B*, 2003, **68**, 212408.
12 S. Foner and S. Hou, *J. Appl. Phys.*, 1962, **33**, 1289–1290.
13 F. C. Fonseca, G. F. Goya, R. F. Jardim, R. Muccillo, N. L. V. Carreno, E. Longo and E. R. Leite, *Phys. Rev. B*, 2002, **66**, 104406.
14 R. K. Zheng, H. Gu, B. Xu and X. X. Zhang, *J. Phys.: Condens. Matter*, 2006, **18**, 5905–5910.
15 S. K. Sharma, J. M. Vargas, E. D. Biasi, F. Béron, M. Knobel, K. R. Pirota, C. T. Meneses, S. Kumar, C. G. Lee, P. G. Pagliuso and C. Rettori, *Nanotechnology*, 2010, **21**, 035602.
16 M. J. Benitez, O. Petracic, H. Tüysüz, F. Schüth and H. Zabel, *Phys. Rev. B*, 2011, **83**, 134424.
17 P. K. Manna, S. M. Yusuf, R. Shukla and A. K. Tyagi, *Phys. Rev. B*, 2011, **83**, 184412.
18 I. S. Jacobs and C. P. Bean, *in Magnetism, edited by G. T. Rado and H. Suhl (Academic Press, New York)*, 1963, **Vol. III**, p. 294.
19 S. D. Tiwari and K. P. Rajeev, *Phys. Rev. B*, 2005, **72**, 104433.
20 D. Gao, G. Yang, J. Li, J. Zhang, J. Zhang and D. Xue, *J. Phys. Chem. C*, 2010, **114**, 18347–18351.
21 G. Yang, D. Gao, Z. Shi, Z. Zhang, J. Zhang, J. Zhang and D. Xue, *J. Phys. Chem. C*, 2010, **114**, 21989–21993.
22 M. Li, S. Ge, W. Qiao, L. Zhang, Y. Zuo and S. Yan, *Appl. Phys. Lett.*, 2009, **94**, 152511.
23 T.-H. Yang, S. Nori, H. Zhou and J. Narayan, *Appl. Phys. Lett.*, 2009, **95**, 102506.
24 G. Z. Xing, J. B. Yi, D. D. Wang, L. Liao, T. Yu, Z. X Shen, C. H. A. Huan, T. C. Sum, J. Ding and T. Wu, *Phys Rev. B*, 2009, **79**, 174406.
25 L. Soriano, M. Abbate, A. Fernández, A. R. González-Elipe, F. Sirotti and J. M. Sanz, *J. Phys. Chem. B*, 1999, **103**, 6676–6679.
26 B. V. Reddy and S. N. Khanna, *Phys. Rev. Lett.*, 1999, **83**, 3170–3173.
27 R. N. Bhowmik, R. Nagarajan and R. Ranganathan, *Phys. Rev. B*, 2004, **69**, 054430.
28 S. A. Makhlouf, *J. Magn. Magn. Mater.*, 2004, **272–276**, 1530–1532.
29 J. O. Artman, J. C. Murphy and S. Foner, *Phys. Rev.*, 1965, **138**, 342–349.
30 T. Nagamiya, *Prog. Theor. Phys.*, 1951, **6**, 342–349.
31 S. Foner, *Phys. Rev.*, 1963, **130**, 183–197.
32 G. N. Rao, Y. D. Yao and J. W. Chen, *IEEE T. MAGN.*, 2005, **41**, 3409–3411.
33 S. A. Makhlouf, H. Al-Allar and R. H. Kodama, *Solid State Commun.*, 2008, **145**, 1–4.